This article has been accepted for publication in a future issue of this journal, but has not been fully edited. Content may change prior to final publication. Citation information: DOI 10.1109/TMI.2018.2868999, IEEE Transactions on Medical Imaging

Dynamic *in vivo* chest x-ray dark-field imaging in mice

R. Gradl, K. S. Morgan, M. Dierolf, C. Jud, L. Hehn, B. Günther, W. Möller, D. Kutschke, L. Yang, T. Stoeger, D. Pfeiffer, B. Gleich, K. Achterhold, O. Schmid, and F. Pfeiffer

***Abstract*—X-ray grating interferometry is a powerful emerging tool in biomedical imaging, providing access to three complementary image modalities. In addition to the conventional attenuation modality, interferometry provides a phase modality that visualises soft tissue structures, and a dark-field modality that relates to the number and size of sub-resolution scattering objects. A particularly strong dark-field signal originates from the alveoli or air sacs in the lung. Dark-field lung radiographs in animal models have already shown increased sensitivity in diagnosing lung diseases such as lung cancer or emphysema, compared to conventional x-ray chest radiography. However, to date, x-ray dark-field lung imaging has either averaged information over several breaths or has been captured during a breath hold. In this report we demonstrate the first time-resolved dark-field imaging of a breath cycle in a mechanically ventilated mouse, *in vivo*, which was obtained using a grating interferometer. We achieved a time resolution of 0.1 s, visualizing the changes in the dark-field, phase and attenuation images during inhalation and exhalation. These measurements show that the dark-field signal depends on the air volume and hence alveolar dimensions of the lung. Conducting this type of scan with animal disease models would help to locate the optimum breath point for single-image diagnostic dark-field imaging, and could indicate if the changes in the dark-field signal during breath provide a diagnostically useful complementary measure.**

***Index Terms*—animal imaging, dark-field and phase-contrast x-ray methods, grating interferometer, lung imaging, x-ray imaging**

Manuscript received July 19, 2018. We acknowledge financial support through the Centre for Advanced Laser Applications (CALA), the DFG Cluster of Excellence Munich-Centre for Advanced Photonics (MAP) and the DFG Gottfried Wilhelm Leibniz program. KM was supported by a Veski VPRF and KM, RG and FP completed this work with the support of the TUM Institute for Advanced Study, funded by the German Excellence Initiative and the European Union Seventh Framework Program under grant agreement no 291763 and co-funded by the European Union. LY received a fellowship from China Scholarship Council (CSC).

R. Gradl and K. S. Morgan contributed equally to this manuscript.

R. Gradl, K. S. Morgan, M. Dierolf, C. Jud, L. Hehn, B. Günther, K. Achterhold and F. Pfeiffer are with the Chair of Biomedical Physics, Department of Physics, Technical University of Munich, James-Franck-Str. 1, 85748 Garching, Germany.

R. Gradl, K. S. Morgan and F. Pfeiffer are with the Institute for Advanced Study, Technical University of Munich, Lichtenbergstr. 2 a, 85748, Garching, Germany

K. S. Morgan is with the School of Physics and Astronomy, Monash University, Clayton, Victoria 3800, Australia

L. Hehn, D. Pfeiffer and F. Pfeiffer are with the Department of Diagnostic and Interventional Radiology, Klinikum rechts der Isar, Technical University of Munich, Ismaninger Str. 22, 81675 München, Germany

B. Günther is with the Max-Planck-Institute of Quantum Optics, Hans-Kopfermann-Str. 1, 85748 Garching, Germany

W. Möller, D. Kutschke, L. Yang, T. Stoeger and O. Schmid are with Comprehensive Pneumology Center, Member of the German Center for Lung Research (DZL), Max-Lebsche-Platz 31, 81377 München, Germany and with the Institute of Lung Biology and Disease, Helmholtz Zentrum München - German Research Center for Environmental Health, Ingolstädter Landstr. 1, 85764 Neuherberg, Germany

[1]

I. Introduction

THE World Health Organization (WHO) states that lung diseases are one of the top ten causes of death globally, with chronic obstructive pulmonary disease and lung cancer claiming a total of 4.9 million lives in 2015 [1]. Characteristic of these diseases is a change in lung epithelium and/or the structure of the alveoli (air sacs), both of which lead to disruption of the $O_2 - CO_2$ exchange. The prognosis for lung diseases is poor, because they are typically diagnosed at an already advanced stage. Current diagnostics are mostly performed by imaging methods such as x-ray chest radiography. These radiographs suffer from limited soft tissue contrast, which is why early stages of lung diseases are often missed. Improved contrast and spatial separation of features is available via chest computed tomography (CT), however this involves a higher radiation dose for the patient. Consequently, chest-CT has limited acceptance as a general screening method at the moment, and the United States Preventive Services Task Force recommends annual lung cancer CT screening only for adults >55 years who have a long-lasting smoking history [2].

Recent studies in grating-based x-ray imaging have shown that the x-ray dark-field signal, which is related to small-angle scattering [3], is a useful tool for imaging lung tissue, since the dark-field signal depends on the number of alveoli and mean alveolar size. When alveoli airspaces increase in volume (e.g. as seen with emphysema), they scatter the x-ray wavefield less and produce a reduced dark-field signal [4], [5]. If the alveoli are clogged up or the alveolar walls are thickened by disease (e.g. as a result of fibrosis or infection), the dark-field signal is reduced. Therefore, an improved discrimination between healthy and diseased tissue is possible by examining this signal [6], [7], [8]. Recently-published small animal studies showed that x-ray dark-field imaging improves the early diagnosis of pulmonary emphysema [4], [7], [6], [9], pulmonary fibrosis [10], lung cancer [11] and pneumothoraces [12]. Furthermore, dark-field x-ray imaging can help to visualize neonatal lung injury induced by mechanical ventilation [13].

This article has been accepted for publication in a future issue of this journal, but has not been fully edited. Content may change prior to final publication. Citation information: DOI 10.1109/TMI.2018.2868999, IEEE Transactions on Medical Imaging

Dark-field x-ray imaging is already moving towards clinical application [8], but it is not yet clear at which part of the breath cycle the images will be most diagnostically useful (e.g. at maximum inflation, after breathing out, or at some other timepoint). In clinical routine, chest radiographs are usually performed at the end of inspiration. Inhaling leads to an inflation of the lungs, and therefore increased transparency in attenuation images, which makes it easier to detect pathologic changes within the lungs like tumours or inflammation. However, there are also reasons to do x-ray imaging of the chest at the end of expiration. Pneumothoraces, for example, are easier to detect when the patient exhales, as it increases the relative volume of the pleural cavity [14]. In addition, reproducibility is higher in images taken at the end of expiration, as the range of possible lung positions is smaller after exhalation than after inhalation. In all previous dark-field small-animal studies, images were captured either over several breaths [6], [7], [9], leading to motion blur in the images, or images were captured in a breath-hold situation [8].

We present here the first dynamic grating-based *in vivo* small animal study of lung tissue. In this study, a range of points across the breath cycle were captured using grating interferometery (see Fig. 1 (a)), providing a dark-field signal that varies as a function of the inhalation-exhalation state of a lung. Changes in dark-field signal were observed over the breath cycle in a consistent way for all three mice measured. This approach could therefore be used to determine the optimum inflation for diagnostic imaging. In addition, dynamic dark-field imaging sequences could reveal how the alveoli expand during the breath, which may provide feedback on the elasticity of alveoli across the lung, to better pinpoint local lung diseases that effect elasticity, like fibrosis or emphysema. These capabilities would not only be useful for diagnostic imaging, but also for medical research where researchers aim to test the efficacy of lung disease treatments, for example, in small animal studies.

Measurements were collected using a grating interferometer [5], [4] (see Fig. 1 (a)), which captures multiple exposures of a sample (e.g. here seven), each at a different relative position of the two gratings. These so-called phase step measurements (Fig. 1 (b)) can be used to reconstruct three imaging modalities - attenuation, differential phase and dark-field (see Fig. 1 (c)). Because the breath cycle is repeated and the mechanical ventilation returns the tissue to the same position with each breath (within tolerance), there are multiple opportunities to capture the multiple exposures required. To resolve different timepoints in the breath cycle without motion blur, short exposures are necessary, hence high x-ray flux. In our case, the flux is delivered by the Munich Compact Light Source (MuCLS), a laboratory-based synchrotron that utilises inverse Compton Scattering to produce a high-flux quasi-monochromatic, low-divergence x-ray beam. This allows an exposure time of 40 ms and a frame rate of 10 fps. This is fast enough to capture different timepoints during the breath, provided the mouse is ventilated at a reduced breathing rate during the relatively short imaging period (40 breaths/min here, while 80 breaths/min is typically used for $in\ vivo$ x-ray phase contrast imaging of the murine respiratory system [15]). Utilizing the multiple opportunities for image capture, we successfully performed dynamic x-ray dark-field imaging of a periodic signal, the breath cycle in an *in vivo* mouse.

II. Methods

Figure 1 (a) shows a sketch of the grating-interferometry set-up at the MuCLS [5], [4], [16]. The lungs produced a strong phase signal, hence the sample was placed in between the gratings to adjust the sensitivity of the interferometer. Images were taken continuously at equidistant timepoints during the imaging period, as shown in Figure 1 (b), while the mouse was ventilated with a small animal ventilator. At each grating position we collected images at a range of timepoints across the breath, with the process repeated over several breaths (three breaths in the case of Figure 1 (b)), enabling averaging to increase the signal-to-noise ratio. The grating G1 was then moved to the next position in the phase stepping scan (our experiment captured seven images at different grating positions in order to reconstruct the dark-field image). At the next grating position, images were again collected over a range of timepoints within the breath, over several breaths. The frequency of ventilation was matched to the image capture frequency so that the lungs returned to almost exactly the same position for an image captured one breath later. Once measurements had been collected at all the grating positions (i.e. a full stepping scan has been completed), the exposures were sorted to enable reconstruction of the dark-field image modality at each point in the breath. First, the multiple breath cycles collected at each grating position were averaged, as shown in the first and second row of Fig. 1 (b). Then the images at the same point of the breath cycle were extracted for each grating position, to form a phase stepping scan for the given lung inflation (second and third row of Fig. 1 (b)). This stepping scan was then used to reconstruct the dark-field image using standard grating-based reconstruction algorithms [3], [17]. Figure 1 (c) displays the resulting reconstructed absorption, phase and dark-field radiographs obtained for one point in the breath.

A. Imaging set-up

Imaging was performed at the Munich Compact Light Source (MuCLS) [18], a special type of laboratory x-ray source that exploits the effect of inverse Compton scattering of infrared laser photons from relativistic electrons to produce quasi-monochromatic x-rays [19], [20], [21], [18]. In this study, an x-ray energy of 25 keV (bandwidth 4%) with flux up to 1.7×10^{10} ph/s was chosen. The Talbot interferometer was placed about 15 m away from the source of the x-rays, providing a beam size of around 60 mm in diameter. The grating interferometer consists of a phase (G1) and absorption grating (G2) (see Fig. 1 (a)). The gratings were produced by the Karlsruhe Nano Micro Facility (KNMF). The phase grating has a period of 4.92 µm and a duty cycle of 0.5, inducing a phase shift of $\pi/2$ using nickel grating lines produced with a height of 4.39 µm. At the first fractional

This article has been accepted for publication in a future issue of this journal, but has not been fully edited. Content may change prior to final publication. Citation information: DOI 10.1109/TMI.2018.2868999, IEEE Transactions on Medical Imaging

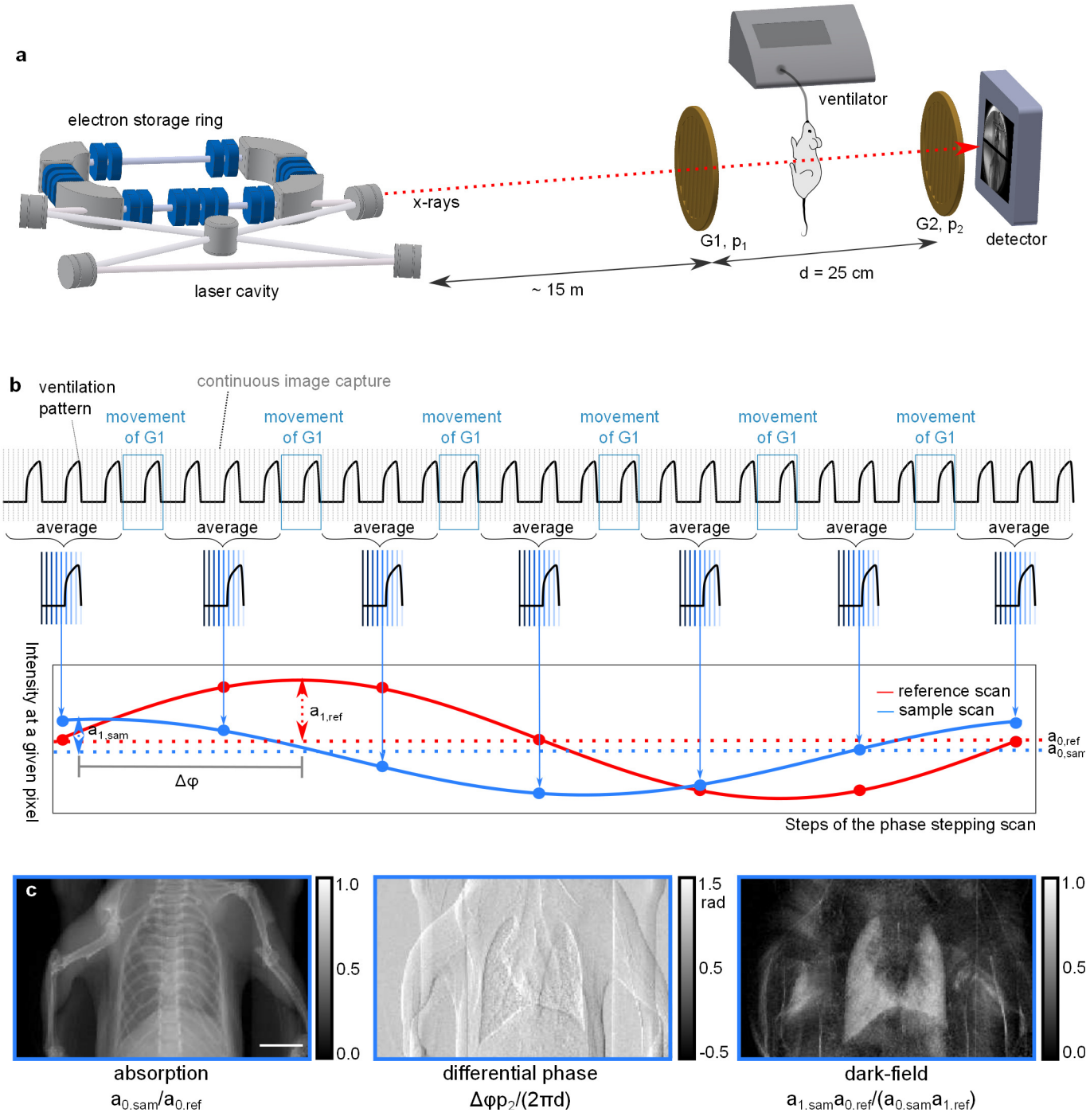

Fig. 1. a) Sketch of the experimental set-up: The mouse is placed in between the gratings of the interferometer and ventilated by a small animal ventilator. b) Sketch of the imaging protocol: Images are taken continuously during the whole imaging period, indicated by vertical lines. The multiple breaths in between each grating movement are averaged to enhance the signal-to-noise ratio. Images from the same point in each breath cycle are then extracted and a phase stepping curve assembled at each pixel. The stepping curve is a sinusoid with a mean value of a_0, an amplitude of a_1 and a relative phase of ϕ, for both a sample scan ('sam') and a reference scan ('ref'), which is taken when no sample is present. These stepping curve parameters are used to reconstruct c) Three image modalities: absorption (the bones are clearly visible), differential phase (the edges of the lung and airways are clearly visible) and dark-field signal (the lungs and the fur of the mouse are most visible). Scalebar: 5 mm.

This article has been accepted for publication in a future issue of this journal, but has not been fully edited. Content may change prior to final publication. Citation information: DOI 10.1109/TMI.2018.2868999, IEEE Transactions on Medical Imaging

Talbot distance, 248 mm downstream of G1, an absorption grating (G2) is placed, with a period of 5 μm and a duty cycle of 0.5. The grating bars are made from gold, with a height of 70 μm [16]. Directly behind the absorption grating, a Pilatus 200K detector (Dectris Ltd., Baden, Switzerland) was placed. This detector has a pixel size of 172 μm, an array size of 487 x 407 pixels and a 1000 μm thick silicon sensor.

The sample was placed in between the gratings and moved out of the beam in order to capture a reference phase stepping scan. The mouse was ventilated by a small animal ventilator (flexiVent FX, SCIREQ) at 40 breaths/min over an 84 s imaging period. Before and after imaging, the mouse was ventilated at 120 breaths/min. The tidal volume was set to 30 ml/kg (mice typically weighed 20 grams), with a pressure limit of 30 hPa. The inspiration-expiration ratio was 75% (inspiratory time 0.64 s, expiratory time 0.86 s, inspiratory breath hold 0 s). Seven grating positions were used for one stepping curve. Images were collected for 9 s at each grating position, with 3 s provided to move the grating to the next position on the stepping curve. Images were collected throughout this time, so that the image capture would maintain the same synchronisation with the breath for all 7 grating positions. Note that the images captured during grating movement were not used for analysis and were discarded. The visibility, which is a key characteristic of a grating set-up, was 40 %. Visibility is defined as $V = (I_{max} - I_{min})/(I_{max} + I_{min})$ = $a_{1,ref}/a_{0,ref}$, with I_{min} and I_{max} the minimum and maximum intensity in a reference phase stepping scan, respectively (see Fig. 1 (b)).
The sensitivity of the interferometer was adjusted by varying the distance between sample and G2 (see Supplementary Fig. 1), and set to 12 cm for the results shown in the body of this paper.
Exposure times of 40 ms, 90 ms and 140 ms, which correspond to 30, 15 and 10 images per breath respectively, were tested during the study. In this report we focus on the results when imaging with 90 ms exposures, because this was the best balance of time resolution and sufficient signal-to-noise ratio. Results for 40 ms and 140 ms can be found in Supplementary Videos 1 and 3. The scan shown in this report was captured for three living mice. The dark-field sequences of all three mice are added in the supplementary material, in all cases using 90 ms exposures. The mean absorbed dose was estimated to be 20 mGy for the total imaging time of 84 s, assuming 25 keV monochromatic x-rays and following the method set out by Boone et al. [22] for a 25 mm mouse diameter (note that the absorption of G1 was neglected). The total delivered dose could be reduced using collimators, so that only the lungs are irradiated and not the whole mouse (as it was the case in this study).

B. Image analysis

Image analysis was performed using in-house software written in Python (Python Software Foundation). To retrieve the three image modalities (absorption, dark-field and differential phase) from the obtained dataset, the data was first sorted so that we had an image of the same point in the breath cycle for all seven grating steps. These images are used to extract a stepping curve (see Fig. 1 (b), blue curve, addedfitted using the 'sam' parameters). To enhance the signal-to-noise ratio, each image in the stepping curve was an average from three consecutive breaths. The reference stepping curve was obtained after the sample scan (see Fig. 1 (b), red curve, fitted using the 'ref' parameters), with 60 flat-field images averaged together at each step. The stepping data was analysed using an expectation-maximization algorithm, which corrects for uncertainties in the stepping positions, to extract the three image modalities [23]. Absorption images are obtained from the ratio of the average value of the sample and reference stepping curves($a_{0,sam}$ / $a_{0,ref}$, see Fig. 1 (b) and caption). The differential phase images come from the phase shift between the stepping curves ($\Delta\varphi p_2$ / (2πd), where p_2 is the period of the second grating and d is the inter-grating distance, see Fig. 1 (b)). Dark-field images are calculated by the sample-induced relative decrease in the normalized visibility introduced by the sample to the stepping curve (($a_{1,sam}$ $a_{0,ref}$) / ($a_{0,sam}$ $a_{1,ref}$), see Fig. 1 (b)) [24].

C. Animal ethics statement

All procedures for animal handling and experiments were performed in accordance with protocols approved by the Regierung von Oberbayern (District Government of Upper Bavaria). Mice were kept in isolated ventilated cages (IVC-Racks; BioZone, Margate) supplied with filtered air in a 12 hr light / 12 hr dark cycle (lights on from 06:00 - 18:00). Food (standard chow) and water were available *ad libitum*.

D. Animal handling

C57BL/6 mice (age 8-14 weeks, female, weight 18-22 g) were anaesthetized by intraperitoneal injection of a mixture of Medetomidine (0.5 mg/kg body mass), Midazolam (5.0 mg/kg body mass) and Fentanyl (0.05 mg/kg body mass). The animals were then intubated by a non-surgical technique [25] with a 20 Ga cannula. Then, the mouse was placed into the hutch for imaging where it was ventilated (flexiVent FX, SCIREQ). Immediately after imaging was completed, the still-anesthetized mice were killed by exsanguination.

III. Results

Different timepoints across one breath are displayed in Figure 2 for the three image modalities; (a) the absorption signal, (b) the differential phase signal, and (c) the dark-field signal. In the differential phase images, the expansion of the airways during inhalation is visible, most easily observed in the supplementary videos. Figure 2 (d) shows the dark-field signal again, this time with pixels binned 2×2 and a colour mapping applied to more easily visualize the changes in the magnitude of the dark-field. 15 images were captured over the 1.5 second breath cycle, with an exposure time of 90 ms and 10 ms between each image, providing a time resolution of 0.1 seconds. This sequence commences at the point of minimum

This article has been accepted for publication in a future issue of this journal, but has not been fully edited. Content may change prior to final publication. Citation information: DOI 10.1109/TMI.2018.2868999, IEEE Transactions on Medical Imaging

lung volume. The lungs beginning to expand 0.8 seconds later, reach maximum air volume at 1.3 seconds, and then the air is exhaled rapidly. This movement, particularly at the lower periphery of the lungs, is clearly visible in all three imaging modalities, particularly in reference to the dotted red outline that corresponds to the start of the breath (see also the movies in the supplementary material). In Fig. 2 (d) the dark-field signal changes are more easily observed, especially in the left lung. In the central part of the left lung, the colour changes from red at full exhalation, to yellow/green at full inhalation (when alveoli are at their maximum volume). An analysis of the segmented lung signal for the left (blue) and right (orange) halves of the lung (see Fig. 3 (a)) is plotted in Fig. 3 (b) for the dark-field signal. The projected area was segmented manually and adapted for each image, so that the area of interest comprises lung tissue only. In the background of the signal plot the ventilation pattern (taken from the flexiVent system) is displayed in grey. The lowest average dark-field signal is observed when the lung is at full inhalation, changing by 3 - 4% of the average dark-field signal (measured in three different mice with identical experimental parameters). Note that the dark-field signal depends almost entirely on the lung tissue, whereas attenuation images include contributions from the lung and of overlying features like the bones. It is also worth noting that the range of dark-field values across the lung (measured here by the standard deviation of the pixel values in the selected area shown in Fig. 3 (a)) was reduced at the maximum air volume, when the lung is more uniformly inflated.

IV. Discussion

The images shown here demonstrate that the dark-field signal generated by a breathing lung does change in a detectable way during the breath cycle. The average dark-field signal across the lung is reduced by 3 - 4 % when the lung is extended and at maximum air volume. This is the point when the alveoli are most enlarged and the number of air/tissue interfaces within a given projected area are at a minimum. This observation is consistent with previous work that measured a reduced dark-field signal in projection when lung disease reduced the number of air/tissue interfaces [7], [10], [8]. A global reduction of around 20% of the maximum lung dark field signal has been observed due to emphysema [7], and a local reduction of 10 - 30% for pulmonary fibrosis [10] and of 10 - 70% for lung cancer [11], in all cases depending on the severity of the disease.

The method described here for dynamic x-ray grating interferometry of repeated motion represents the first dynamic x-ray dark-field imaging, and achieves this *in vivo*. While this is the first time-resolved study to look at the dark-field signal, previous work has captured a time-resolved phase signal. Time-resolved x-ray phase contrast tomography with a Talbot interferometer has been published using high-flux synchrotron sources, via the Moire approach [26], [27], [28]. In this approach, gratings are rotated to create resolvable Moire fringes at the detector and extract a phase signal, typically at a slightly reduced spatial resolution. In these experiments, fast imaging was achieved using white beam synchrotron radiation. Differential phase images have also been captured using phase-stepping to utilise the full spatial resolution of the detector, both in projection [29] (repeating the motion of the PMMA sample to create multiple opportunities for image capture), and in tomography [30], [31] (mechanically stretching a pig aorta and a rat tail).

We optimised two key experimental parameters to achieve the required temporal resolution and imaging sensitivity to capture the moving lungs. To allow for fast imaging, short exposure times are required. With a longer exposure time, the signal-to-noise ratio in the reconstructed images can be increased, however the time resolution across the breath is decreased. We tested exposure times of 40 ms, 90 ms and 140 ms, which allowed for 30, 15 and 10 images across the breath cycle respectively, with increased noise visible at the shorter exposure times. These images are provided in Supplementary Videos 1, 2 and 3, respectively. The signal-to-noise ratio could be increased independently of exposure time by capturing more breath cycles at each grating position, at the expense of increased radiation dose. Also note if the images are collected *in vivo* at a reduced breathing rate compared to normal, as is the case here, the total available imaging time is physiologically limited. The sensitivity of the set-up was also considered in this experiment. Because the lungs produce such strong phase and dark-field signals, the mouse had to be placed relatively close to G2, tuning the sensitivity to ensure that the dark-field signal would not saturate and produce erroneous pixels in the differential phase image (we kept the dark-field signal <0.9). Supplementary Figure 1 shows the results of tuning the interferometer sensitivity.

The images shown in this report could be further improved in future studies. Firstly, a high-resolution detector could be used, as long as exposure times are still compatible with the image acquisition protocol. In this scenario, the projected lung image just occupied a small part of the detector field-of-view, an area of only about 100 pixels wide. If a higher-resolution detector was used, so that the lung image filled the detector field-of-view, we could access an area closer to several thousand pixels in width (as seen in propagation-based phase contrast lung imaging at the same source [32]). An increased spatial resolution would allow us to better examine the regional dark-field signal and spatial variations in dark-field signal (e.g. monitoring the standard deviation of the dark-field signal across an area of the lung during the breath). A second area for improvement is the significant x-ray dark-field signal produced by the fur of the mouse, seen particularly on the left of the dark field image in Fig. 1 (c), both on the shoulder and where the fur is compressed under the arm. The fur of the mouse could be removed from the area of interest or nude mice could be used, which would isolate the scattering signal from the lungs more clearly. Thirdly, it would be possible to capture the lungs moving at a faster breathing rate than used here, if additional x-ray flux were available and hence the exposure times could be decreased. Note that the flux density of the MuCLS during this experiment, for this field-of-view, was no greater than that of a rotating anode x-ray source, meaning that this kind and rate

This article has been accepted for publication in a future issue of this journal, but has not been fully edited. Content may change prior to final publication. Citation information: DOI 10.1109/TMI.2018.2868999, IEEE Transactions on Medical Imaging

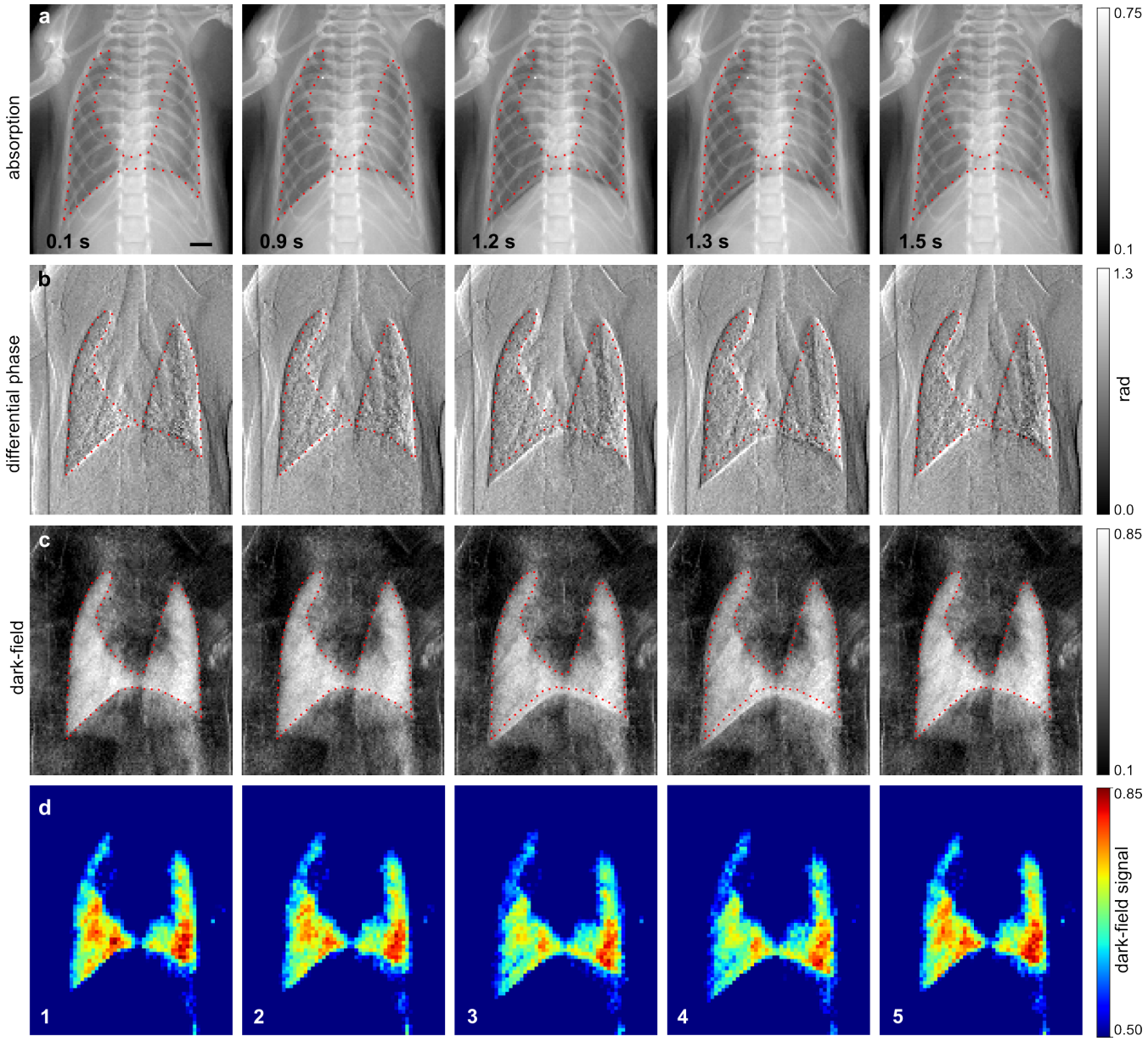

Fig. 2. a) The absorption, b) differential phase, c) dark-field and d) 2x2 spatially-binned dark-field images (shown with a colour look-up table), each at five timepoints across the breath cycle. The red dotted outline in a, b and c is fixed at full exhalation to highlight the changes in the shape of the lung during inhalation. The white numbers in d correlate to the points in the breath cycle highlighted in Fig. 3 (b). Movie sequences for each imaging modality at all fifteen timepoints are included in Supplementary Video 2. Scalebar: 2 mm.

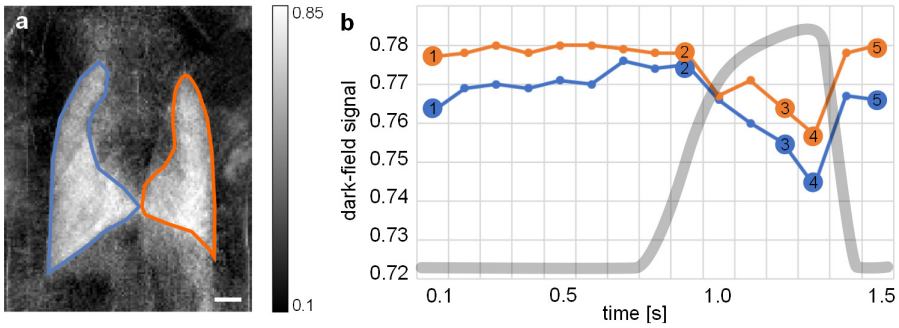

Fig. 3. a) The left (blue) and right (orange) lobe of the lung were selected manually, and the area adapted for each timepoint. b) The mean dark-field value was then plotted for the lobes, as a function of time. The shape of the breath cycle is shown in gray in the background of the plot (provided by the flexiVent ventilation system software). Scalebar: 2 mm.

of imaging could be conducted at conventional x-ray sources. In the case of a conventional x-ray source, where the spot-size is usually larger, a third grating (G0) would be placed between the source and grating G1 to increase the observed coherence [33]. While the sensitivity of the system may be affected by the spot-size and polychromaticity, the very strong dark field signal seen from the lungs means that this kind of experiment would be feasible.

The dose delivered to the sample could be reduced by either performing less phase steps for the stepping scan (e.g. three steps), or less breaths per step for averaging. However, the resulting increased sensitivity to noise and the increased difficulty of image reconstruction seen from less images mean that to have a net benefit, advanced reconstruction or de-noising algorithms should be employed (e.g. using the similarity of consecutive frames). Unless dose must be minimised, for example, to enable repeat imaging, we suggest the protocol outlined in this experiment. The experiment would also naturally benefit from a detector with increased efficiency and grating structures with thinner substrates that let more of the x-ray flux through to the sample.

Future studies will compare the change in the dynamic dark-field signal between healthy and diseased lungs. These kind of time-resolved studies can determine the best point in the breath for single-projection diagnostic imaging for a given pathology. Giving the pathophysiological changes in emphysema and fibrosis, the dark-field-time curve, or even simply the ratio of dark-field signals at maximum inhalation and exhalation, will provide additional information on the local capability of the lung issue to inflate and deflate during the breathing cycle. Such a ratio may serve as a future non-invasive biomarker of pulmonary function and will provide better differentiation and detection of lung disease, particularly where the elasticity of the alveoli is affected.

V. Conclusion

The X-ray grating interferometer has recently gained interest as a potential diagnostic tool for lung disease, visualising differences in lung structure both globally (e.g. emphysema) and locally (e.g. lung cancer) via the dark-field signal. This signal relates to the number and size of sub-resolution structures, and hence reveals properties of the air sacs in the lungs, and would be expected to change through the breath cycle. Here we have shown the first time-resolved dark-field chest radiographs, captured with living mice. The changes observed here in the dark-field signal as the air sacs inflate indicate that this approach can provide not only structural, but also functional information on lung health.

Acknowledgment

The MuCLS was developed and constructed by Lyncean Technologies Inc and we thank Lyncean for their support operating the MuCLS. This work was carried out with the support of the Karlsruhe Nano Micro Facility (KNMF, www.kit.edu/knmf), a Helmholtz Research Infrastructure at Karlsruhe Institute of Technology (KIT).

References

[1] WHO. (2017) The top 10 causes of death. Accessed 25-Nov-2017. [Online]. Available: http://www.who.int/mediacentre/factsheets/fs310/en/

[2] US Preventive Services Task Force . (2013) Screening for Lung Cancer. Accessed 02-Mar-2018. [Online]. Available: https://www.uspreventiveservicestaskforce.org/Page/Document/UpdateSummaryFinal/lung-cancer-screening

[3] F. Pfeiffer, M. Bech, O. Bunk, P. Kraft, E. F. Eikenberry, C. Brönnimann, C. Grünzweig, and C. David, "Hard-X-ray dark-field imaging using a grating interferometer." *Nature Materials*, vol. 7, pp. 134–137, 2008.

[4] S. Schleede, F. G. Meinel, M. Bech, J. Herzen, K. Achterhold, G. Potdevin, A. Malecki, S. Adam-Neumair, S. Thieme, F. Bamberg, K. Nikolaou, A. Bohla, A. Yildirim, R. Loewen, M. Gifford, R. Ruth, O. Eickelberg, M. Reiser, and F. Pfeiffer, "Emphysema diagnosis using X-ray dark-field imaging at a laser-driven compact synchrotron light source," *PNAS*, vol. 109, no. 44, pp. 17 880–17 885, 2012.

[5] M. Bech, O. Bunk, C. David, R. Ruth, J. Rifkin, R. Loewen, R. Feidenhans'l, and F. Pfeiffer, "Hard X-ray phase-contrast imaging with the Compact Light Source based on inverse Compton X-rays," *Journal of Synchrotron Radiation*, vol. 16, pp. 43–47, Jan 2009.

[6] F. G. Meinel, F. Schwab, S. Schleede, M. Bech, J. Herzen, K. Achterhold, S. Auweter, F. Bamberg, A. Ö. Yildirim, A. Bohla, O. Eickelberg, R. Loewen, M. Gifford, R. Ruth, M. F. Reiser, F. Pfeiffer, and K. Nikolaou, "Diagnosing and Mapping Pulmonary Emphysema on X-Ray Projection Images: Incremental Value of Grating-Based X-Ray Dark-Field Imaging," *PLoS One*, vol. 3, no. 8, p. e59526, 2013.

[7] A. Yaroshenko, F. G. Meinel, M. Bech, A. Tapfer, A. Velroyen, S. Schleede, A. Bohla, A. A. Ö. Yildirim, K. Nikolaou, O. Eickelberg, M. F. Reiser, S. Auweter, F. Bamberg, and F. Pfeiffer, "Pulmonary emphysema diagnosis with a preclinical small-animal x-ray dark-field scatter-contrast scanner," *Radiology*, vol. 269, no. 2, pp. 427–433, 2013.

[8] L. B. Gromann, F. De Marco, K. Willer, P. B. Noël, K. Scherer, B. Renger, B. Gleich, K. Achterhold, A. A. Fingerle, D. Muenzel, S. Auweter, K. Hellbach, M. Reiser, A. Baehr, M. Dmochewitz, T. J. Schroeter, F. J. Koch, P. Meyer, D. Kunka, J. Mohr, A. Yaroshenko, H. I. Maack, T. Pralow, H. Van Der Heijden, R. Proksa, T. Koehler, N. Wieberneit, K. Rindt, E. J. Rummeny, F. Pfeiffer, and J. Herzen, "In-vivo X-ray Dark-Field Chest Radiography of a Pig," *Scientific Reports*, vol. 7, no. 4807, p. 4807, 2017.

[9] K. Hellbach, A. Yaroshenko, F. G. Meinel, A. Ö. Yildirim, T. M. Conlon, M. Bech, M. Mueller, A. Velroyen, M. Notohamiprodjo, F. Bamberg, S. Auweter, M. Reiser, O. Eickelberg, and F. Pfeiffer, "In Vivo Dark-Field Radiography for Early Diagnosis and Staging of Pulmonary Emphysema," *Investigative Radiology*, vol. 50, no. 7, pp. 430–435, 2015.

[10] A. Yaroshenko, K. Hellbach, A. Ö. Yildirim, T. M. Conlon, I. E. Fernandez, M. Bech, A. Velroyen, F. G. Meinel, S. Auweter, M. Reiser, *et al.*, "Improved in vivo assessment of pulmonary fibrosis in mice using x-ray dark-field radiography," *Scientific Reports*, vol. 5, p. 17492, 2015.

[11] K. Scherer, A. Yaroshenko, D. A. Bölükbas, L. B. Gromann, K. Hellbach, F. G. Meinel, M. Braunagel, J. Von Berg, O. Eickelberg, M. F. Reiser, F. Pfeiffer, S. Meiners, and J. Herzen, "X-ray Dark-field Radiography - In-Vivo Diagnosis of Lung Cancer in Mice," *Scientific Reports*, vol. 7, no. 402, p. 402, 2017.

[12] K. Hellbach, A. Yaroshenko, K. Willer, T. Pritzke, A. Baumann, N. Hesse, S. Auweter, M. Reiser, O. Eickelberg, F. Pfeiffer, A. Hilgendorff, and F. Meinel, "Facilitated Diagnosis of Pneumothoraces in Newborn Mice Using X-ray Dark-Field Radiography," *Investigative Radiology*, vol. 51, no. 10, pp. 597–601, 2016.

[13] A. Yaroshenko, T. Pritzke, M. Koschlig, N. Kamgari, K. Willer, L. Gromann, S. Auweter, K. Hellbach, M. Reiser, O. Eickelberg, F. Pfeiffer, and A. Hilgendorff, "Visualization of neonatal lung injury associated with mechanical ventilation using x-ray dark-field radiography," *Scientific Reports*, vol. 6, no. April, p. 24269, 2016.

[14] J. S. Benseler, *The radiology handbook : a pocket guide to medical imaging*, ser. White coat pocket guide. Ohio University Press, 2006.

[15] M. Donnelley, D. Parsons, K. Morgan, and K. Siu, "Animals in synchrotrons: Overcoming challenges for high-resolution, live, small-animal imaging," *AIP Conference Proceedings*, vol. 1266, no. 1, pp. 30–34, 2010.

[16] C. Jud, E. Braig, M. Dierolf, E. Eggl, B. Günther, K. Achterhold, B. Gleich, E. Rummeny, P. Noël, F. Pfeiffer, and D. Muenzel, "Trabecular bone anisotropy imaging with a compact laser-undulator synchrotron x-ray source," *Scientific Reports*, vol. 7, p. 14477, 2017.

[17] Z. Wang and B. Han, "Advanced iterative algorithm for phase extraction of randomly phase-shifted interferograms," *Optics Letter*, vol. 29, no. 14, pp. 1671–1673, Jul 2004.
[18] E. Eggl, M. Dierolf, K. Achterhold, C. Jud, B. Günther, E. Braig, B. Gleich, and F. Pfeiffer, "The Munich Compact Light Source: initial performance measures," *Journal of Synchrotron Radiation*, vol. 23, no. 5, pp. 1137–1142, 2016.
[19] E. Esarey, S. K. Ride, and P. Sprangle, "Nonlinear Thomson scattering of intense laser pulses from beams and plasmas," *Physical Review E*, vol. 48, pp. 3003–3021, Oct 1993.
[20] S. K. Ride, E. Esarey, and M. Baine, "Thomson scattering of intense lasers from electron beams at arbitrary interaction angles," *Physical Review E*, vol. 52, pp. 5425–5442, Nov 1995.
[21] J. R. Loewen, "A compact light source: Design and technical feasibility study of a LASER-electron storage ring X-ray source," Ph.D. dissertation, SLAC-Report-632, Stanford University, 2003.
[22] J. M. Boone, O. Velazquez, and S. R. Cherry, "Small-Animal X-ray Dose from Micro-CT," *Molecular Imaging*, vol. 3, no. 3, pp. 149–158, 2004.
[23] M. Marschner, M. Willner, G. Potdevin, A. Fehringer, P. B. Noël, F. Pfeiffer, and J. Herzen, "Helical X-ray phase-contrast computed tomography without phase stepping," *Scientific Reports*, vol. 6, p. 23953, 2016.
[24] F. Pfeiffer, M. Bech, O. Bunk, T. Donath, B. Henrich, P. Kraft, and C. David, "X-ray dark-field and phase-contrast imaging using a grating interferometer," *Journal of Applied Physics*, vol. 105, no. 10, p. 102006, 2009.
[25] N. Barapatre, P. Symvoulidis, W. Mller, F. Prade, N. Deliolanis, S. Hertel, G. Winter, A. Ö. Yildirim, T. Stoeger, O. Eickelberg, V. Ntziachristos, and O. Schmid, "Quantitative detection of drug dose and spatial distribution in the lung revealed by Cryoslicing Imaging," *Journal of Pharmaceutical and Biomedical Analysis*, vol. 102, pp. 129–136, 2015.
[26] A. Momose, W. Yashiro, S. Harasse, and H. Kuwabara, "Four-dimensional X-ray phase tomography with Talbot interferometry and white synchrotron radiation: dynamic observation of a living worm," *Optics Express*, vol. 19, no. 9, pp. 8423–8432, 2011.
[27] M. P. Olbinado, S. Harasse, W. Yashiro, and A. Momose, "X-ray Talbot-Lau Interferometer for High-Speed Phase Imaging and Tomography Using White Synchrotron Radiation," *AIP Conference Proceedings*, vol. 1466, pp. 266–271, 07 2012.
[28] W. Yashiro, D. Noda, and K. Kajiwara, "Sub-10-ms X-ray tomography using a grating interferometer," *Applied Physics Express*, vol. 10, no. 5, p. 052501, 2017.
[29] M. P. Olbinado, P. Vagovič, W. Yashiro, and A. Momose, "Demonstration of stroboscopic X-ray talbot interferometry using polychromatic synchrotron and laboratory X-ray sources," *Applied Physics Express*, vol. 6, no. 9, p. 096601, 2013.
[30] M. Hoshino, K. Uesugi, T. Tsukube, and N. Yagi, "Quantitative and dynamic measurements of biological fresh samples with X-ray phase contrast tomography," *Journal of Synchrotron Radiation*, vol. 21, no. 6, pp. 1347–1357, 2014.
[31] M. Hoshino, K. Uesugi, and N. Yagi, "4d x-ray phase contrast tomography for repeatable motion of biological samples," *Review of Scientific Instruments*, vol. 87, no. 9, p. 093705, 2016.
[32] R. Gradl, M. Dierolf, K. Achterhold, B. Günther, B. Gleich, F. Pfeiffer, and K. Morgan, "Propagation-based X-ray phase-contrast Imaging at a Compact Light Source," *Scientific Reports*, vol. 7, no. 4908, 2017.
[33] F. Pfeiffer, T. Weitkamp, O. Bunk, and C. David, "Phase retrieval and differential phase-contrast imaging with low-brilliance x-ray sources," *Nature physics*, vol. 2, no. 4, p. 258, 2006.